

Diagnosis of CO Pollution in HTPEM Fuel Cell using Statistical Change Detection

Christian Jeppesen * Mogens Blanke **,*** Fan Zhou *
Søren Juhl Andreassen *

* *Department of Energy Technology, Aalborg University, 9220 Aalborg, Denmark (e-mail: chj@et.aau.dk)*

** *Department of Electrical Engineering, Technical University of Denmark, 2800 Kgs. Lyngby, Denmark, (e-mail: mb@elektro.dtu.dk)*

*** *AMOS CoE, Institute of Technical Cybernetics, Norwegian University of Science and Technology, Trondheim, Norway*

Abstract: The fuel cell technologies are advancing and maturing for commercial markets. However proper diagnostic tools needs to be developed in order to insure reliability and durability of fuel cell systems. This paper presents a design of a data driven method to detect CO content in the anode gas of a high temperature fuel cell. In this work the fuel cell characterization is based on an experimental equivalent electrical circuit, where model parameters are mapped as a function of the load current. The designed general likelihood ratio test detection scheme detects whether a equivalent electrical circuit parameter differ from the non-faulty operation. It is proven that the general likelihood ratio test detection scheme, with a very low probability of false alarm, can detect CO content in the anode gas of the fuel cell.

Keywords: Change detection, GLRT, Fault Diagnosis, PEM Fuel Cell, HTPEM, EIS

1. INTRODUCTION

Proton exchange membrane (PEM) fuel cells have been predicted to have a promising future in applications such as auxiliary power, backup power, etc. where gasoline or diesel generators used to be the preferred electricity generator. Fuel cells are appealing in areas with high air pollution, since fuel cells can be operated without particle emissions in the exhaust gas. This is an important property since in many major cities around the world, are introducing regulations on particle emissions, such as NO_x and SO_2 etc. Fuel cells could be a solution to designing an energy system without particle emissions. (Ellis et al., 2001)

The majority of commercial fuel cell applications use low temperature PEM fuel cells, which is one of the most advanced fuel cell technologies, however it often requires an advanced humidity control system for the membrane. If the membrane is too humidified the membrane will flood, and thereby reduce the gas flow. If the humidity gets too low, the membrane will dry out, and this will also reduce the performance of the fuel cell. (Lottin et al., 2009)

To overcome this problem, the temperature of the fuel cell can be raised to above 100 °C. Thereby the water evaporate, and the water management is not an issue any more. To achieve this, the membrane material is changed to for example a polybenzimidazole (PBI) based polymer doped with phosphoric acid. The increase in temperature also yields a raise in electrochemical kinetic rates. This has the benefit that the fuel cell becomes more tolerant to impurities in the gas composition.

High temperature PEM (HTPEM) fuel cells are therefore often used in combination with a natural gas or methanol reformer. Reformed gas often contains CO, (Justesen et al., 2013) which at too high concentrations damage the fuel cell, but can maintain normal operation at low concentrations of CO in the anode gas. It is therefore desirable to detect small concentration variations in the CO anode gas concentration.

Very little in the literature have done in the area of detecting CO in the anode gas of HTPEM fuel cells. In (Andreassen et al., 2011) and others the effect on the fuel cell impedance when introducing CO and CO_2 in the anode gas was investigated. In (Beer et al., 2013) the author investigates the effect of CO in the anode gas on an extended equivalent electrical circuit, where an dedicated fault element is introduced. In (Jensen et al., 2013) the amount of CO was estimated by examining the fuel cell impedance at 100 Hz.

The purpose of this paper is to develop a methodology for indirect detection of CO in the anode gas, of a high temperature fuel cell. The paper first characterize normal fuel cell behavior, mainly seen through the electrical impedance of the fuel cell under non-faulty conditions and under variations in load current, and based on this, developing a equivalent electrical circuit parameter estimation as a function of the load current. Statistical properties are investigated for the non-faulty state, and based on that a generalized likelihood ratio test (GLRT) is implemented, and proven suitable for this diagnostic problem. A change detection scheme that can detect when

a CO concentration in anode gas begins to reach a level, where the cell could develop non-reversible degradation which will lead to a lifetime reduction which will require timely demanding maintenance of the fuel cell system. A detection scheme that detects a high level of CO in the anode gas could therefore shutdown the fuel cell system before it gets damaged, or change operating conditions in the hydrogen supplying reformer in order to reduce the CO contamination.

2. FUEL CELL CHARACTERIZATION AND EQUIVALENT MODEL

For characterization of fuel cells the most popular method by far, based on the number of publications, is electrochemical impedance spectroscopy (EIS). In galvanostatic EIS a small AC current signal, of known frequency and amplitude, is applied to the fuel cell. The resulting amplitude and phase of the voltage is measured, and the experiment is repeated for a wide sweep of frequencies. From the frequency data, the impedance can be calculated, and plotted in a Bode plot or Nyquist plot. In Fig. 1 is an example of a Nyquist plot shown, where the impedance spectra for a typical PEM fuel cell with one arc, where the frequencies decrease from left to right.

Based on the impedance data, the parameters of an equivalent electric circuit (EEC) network can be fitted, and thereby the impedance data can be quantified into electric component parameters. Many different EEC have been proposed, for PEM fuel cells, and some of the have been adopted for HTPEM fuel cells as in (Andreasen et al., 2009). In this paper, a simplified Randle's EEC is utilized, where only one arc is included. This is done since the impedance response of the fuel cell used in this work is rather simple. A simpler EEC also reduces the fitting time, which is convenient for online diagnostic purpose.

The EEC used in this work is shown in Fig. 1, where the impedance response for a small L_1 is shown in same figure. In order to incorporate mass transport phenomenons and the adsorption of CO in the electrochemical reaction, the capacitor in the Randle's EEC is modeled as a constant phase element (CPE). Furthermore it has been found necessary to get a suitable fit. The impedance response for a CPE, is represented as follows:

$$z_{CPE}(\omega, C_1, \alpha) = \frac{1}{C_1(j\omega)^\alpha} \quad (1)$$

It was proven in (Yang, 2014) that EEC parameter estimation can be done effectively by evolutionary optimization algorithms such as Differential evolution (Storn and Price, 1997). The Differential evolution optimization algorithm is adapted, to fit the acquired impedance data to the EEC shown in Fig 1.

3. EXPERIMENTAL SETUP

The tests were conducted using a single BASF prototype Celtec P2100 HTPEM fuel cell, designed for reformat gas. The active fuel cell area is 45 cm^2 , and was operated at $160 \text{ }^\circ\text{C}$ by electric heaters and waste heat from the fuel cell. The fuel cell was installed in a G60 800 W Greenlight

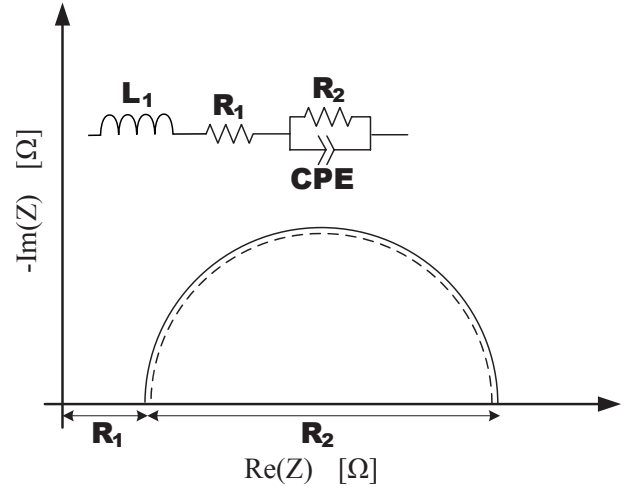


Fig. 1. Nyquist plot for a HTPEM fuel cell, with corresponding equivalent model.

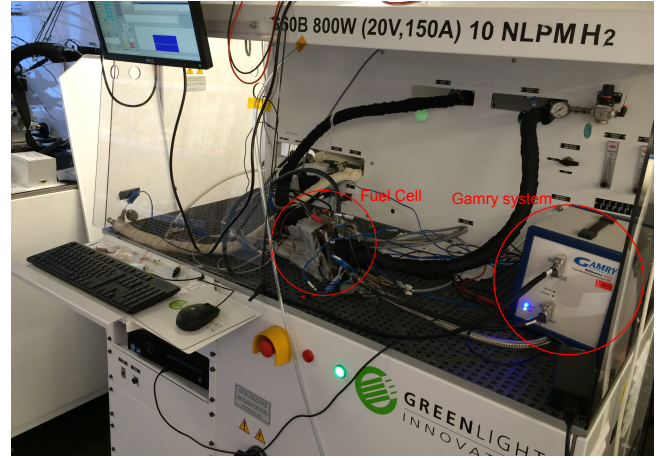


Fig. 2. Test setup used for the experiment. In the left and right circle, the fuel cell assembly and the Gamry system are shown, respectively.

fuel cell test station, where the concentration of CO in the anode gas can be controlled. The experiment set-up is shown in Fig. 2.

Before the experiment, the fuel cell was operated in a break-in procedure for 100 hr at 0.2 A/cm^2 , as an activation procedure in order to achieve a state of equilibrium between the phosphorus acid and the platinum in the membrane.

The break-in and the experiment was conducted by an air stoichiometry of $\lambda_{\text{air}} = 4$ and a hydrogen stoichiometry of $\lambda_{\text{H}_2} = 2.5$. The experiment was performed at a load current of 10 A .

The EIS measurements are performed using a Gamry Reference 3000 instrument running in galvanostatic mode, in a frequency range from 10 kHz to 0.1 Hz , with 20 data points per decade. During the entire CO experiment an EIS measurement is conducted every 20 min . This is also shown in Fig. 5, where it is clearly seen that a change in voltage amplitude occurs every 20 min . This change in voltage amplitude occurs due to the overlaid small amplitude AC current. The duration of one EIS measurement is approximately 4.5 min .

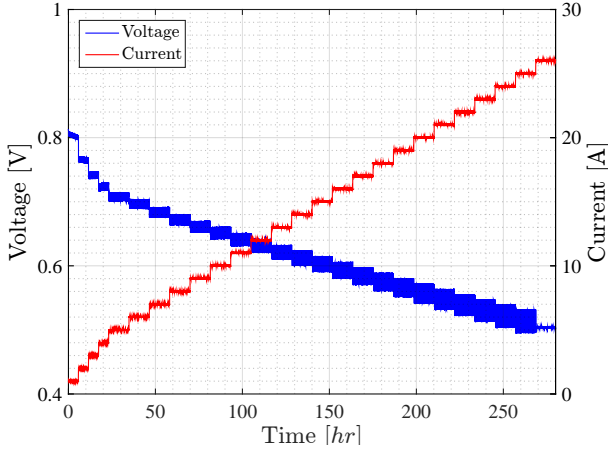


Fig. 3. The voltage polarization profile from the EEC parameters mapping experiment.

4. SYSTEM ANALYSIS

Since the impedance is used as a model for the fuel cell, it is necessary to know how the EEC parameters vary, at different operating conditions. Their value depends on different parameters such as the current, temperature, contamination of the anode and cathode gas, etc. as shown in (Andreasen et al., 2009). This is also why the EEC parameters can be used for change detection.

4.1 Experiment to characterize \mathcal{H}_0 conditions

This therefore requires some pre knowledge on how the EEC parameters vary, as a function on the current and temperature. However, the temperature is kept constant at all time during operation, and therefore the change in EEC parameters as a function of the temperature is neglected. In order to map the EEC parameters as a function of the current, an experiment is conducted in order to identify this mapping. The fuel cell impedance is measured from 1 A to 4 A for 6 hours, and from 5 A to 25 A for 12 hours, with an impedance measurement every 10 minutes. This results in an 11.5 days experiment. The experiment is conducted without any CO contamination in the anode gas. The current and voltage profile is shown in Fig. 3. For every individual impedance measurement, the EEC parameters are estimated using a Differential evolution optimization algorithm. For every current set point, all the EEC parameters are averaged, giving values for each current set point. The average EEC parameters is shown in Fig. 4.

The EEC parameters have a uniform variance at all set points. The mean the variance at each setpoint for R_1 is $\sigma_{R_1}^2 = 1.6 \cdot 10^{-8}$, for R_2 is $\sigma_{R_2}^2 = 3.5 \cdot 10^{-6}$, for C_1 is $\sigma_{C_1}^2 = 2.4 \cdot 10^{-2}$, for α_1 is $\sigma_{\alpha_1}^2 = 1.8 \cdot 10^{-8}$. It is therefore seen that the dispersion of R_1 , R_2 and α_1 is very low, which is convenient for the application of fault detection.

The average EEC parameters in normal operation (no CO contamination in anode gas) is shown in Fig. 4, are fitted using a power function, as shown in eq. 2.

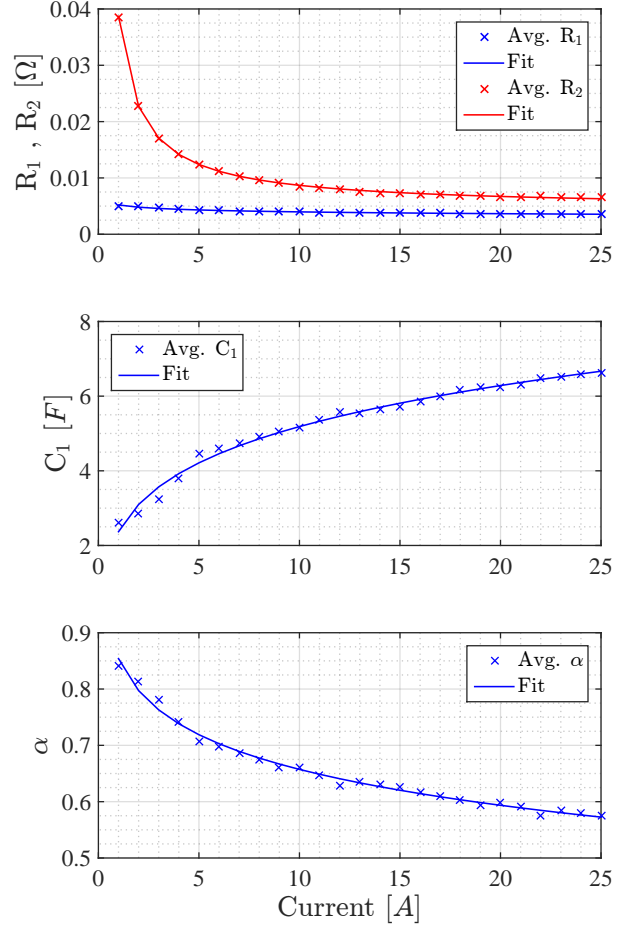


Fig. 4. The EEC parameters as function of the current. The experiment is conducted at 160 °C with pure hydrogen as anode gas. $\lambda_{H_2} = 2.5$ and $\lambda_{air} = 4$.

Table 1. Parameters for the EEC model mapping as a function of the current.

	a	b	c
R_1	0.006204	-0.09585	-0.001004
R_2	0.03421	-0.9097	0.004472
C_1	5.583	0.1774	-3.215
α	-1.631	0.04947	2.485

$$\{R_1, R_2, C_1, \alpha\} = a \cdot \bar{I}^b + c \quad (2)$$

The power function parameters giving the mapping between the steady state current and the EEC parameters, are listed in Table 1. For this mapping to be accurate, it is important that the current used in Eq. 2 is the steady state current. It is therefore suggested that \bar{I} the average current during the time span of an impedance measurement, or a longer period.

4.2 Experiment to characterize \mathcal{H}_1 conditions

In order to obtain the statistical basis for the change detection scheme of the CO content in the anode gas, an experiment has been conducted. The fuel cell is operated 24 hours in normal operation with no CO present in the anode gas with a load of 10 A. This base test will form the basis of a statistical analysis of the non-faulty

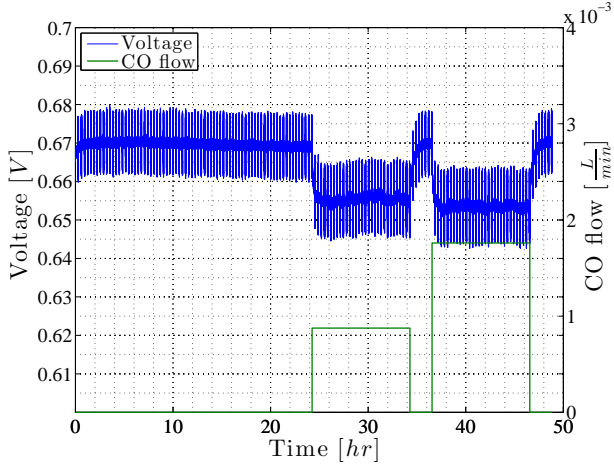


Fig. 5. Fuel cell voltage during the experiment. After 24 hours 0.5% of CO is introduced in the gas, and after 36 hours 1% of CO is introduced in the gas.

operation. In the first 24 hours, an EIS measurement will be conducted every 20 minutes, giving a total of 72 unique model parameter sets. Based on this data an estimation of a probability density function (PDF) for the non-faulty operation will be estimated.

After the first period at normal operation, a concentration of 0.5% CO will be mixed into the anode gas, and the system will operate at 10 hours, with an EIS measurement every 20 minutes. After the first period with CO mixed into the anode gas, a small period of 2 hours without CO mixed into the gas followed by a 10 hours period with 1% of CO mixed into the anode gas. In Fig. 5 the actual volume flow of CO is illustrated by the green line.

As shown in Fig. 5 the CO flow for 0.5% contamination corresponds to less than $1 \frac{mL}{min}$ at $10 A$ and $\lambda_{H_2} = 2.5$, which is the lower limit of the CO mass flow controller. The fuel cell can therefore not be tested at lower contamination rates.

In Fig. 5 it can clearly be seen that when CO is introduced, the fuel cell is rapidly losing performance, by means of a reduction in the cell voltage.

The change in performance can also clearly be seen in Fig. 6. The red data shows the fuel cell impedance without CO mixed into the anode gas, and the blue data shows the impedance with 0.5% CO mixed into the anode gas. It is clearly seen that by introducing CO in the anode gas, the impedance is spread. This corresponds with previously published work. (Araya et al., 2012)

The changes in EEC parameters over time are given in Fig. 7. The first step in CO concentration is introduced at sample nr. 74. As seen in Fig. 7 the parameters R_2 and α indicates evident detectability, when the fault is introduced. The parameter R_1 remains constant when CO is introduced and the C_1 parameter changes when CO is introduced but with slower dynamics.

In Fig. 7 it is seen that the amplitude change for R_2 and α not is the same, for the two different CO concentrations. It can therefore be concluded, that when designing a detection scheme, for an arbitrary change in CO concentration, it have to detect a change with unknown amplitude.

Examining Fig. 7 it is seen that a detection scheme designed to detect on parameter R_2 or α will yield strong

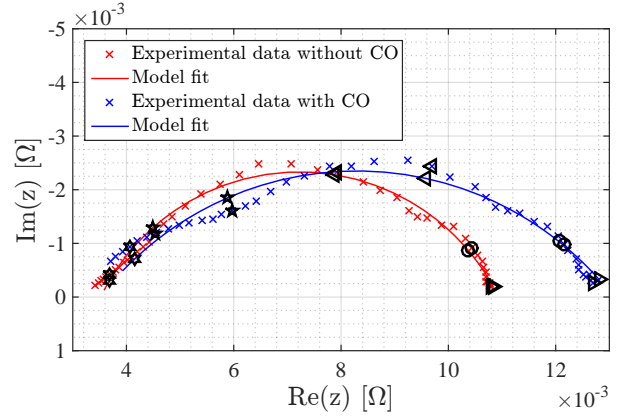


Fig. 6. Impedance data and EEC model fit for operation without CO (red) and with 0.5% CO in the anode gas (blue). The markers indicate the frequency decades.

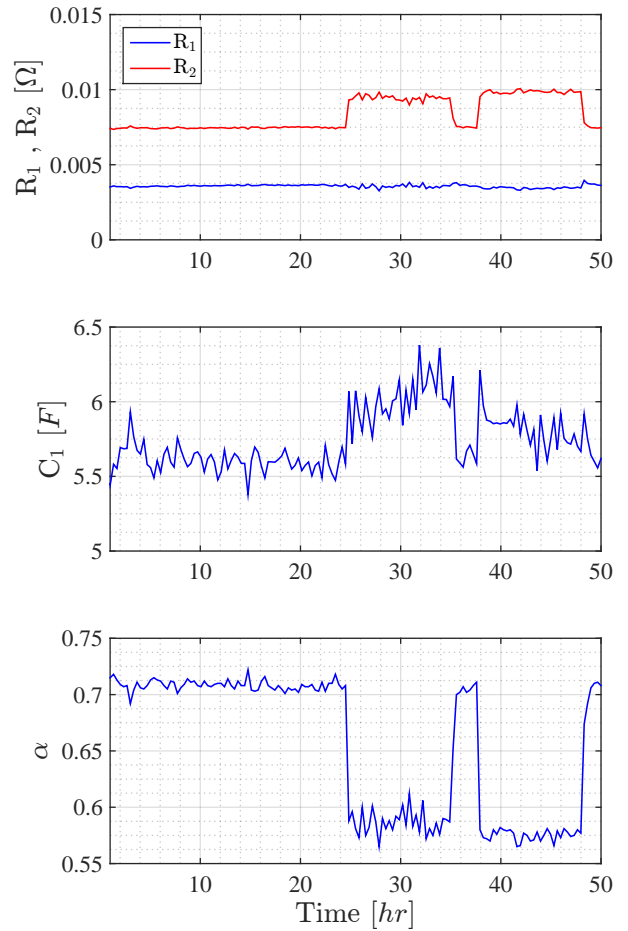


Fig. 7. The EEC parameters as function of time. The experiment is conducted at $160 \text{ }^\circ\text{C}$ and $10 A$ with different CO concentrations mixed into the hydrogen. $\lambda_{H_2} = 2.5$ and $\lambda_{air} = 4$.

detectability of a steady injection of CO in the anode gas. The parameter R_2 is chosen to be the driving parameter in the design of the detection scheme.

The best distribution that fits the data of the parameter R_2 , before the CO is introduced, is a Gaussian distribution

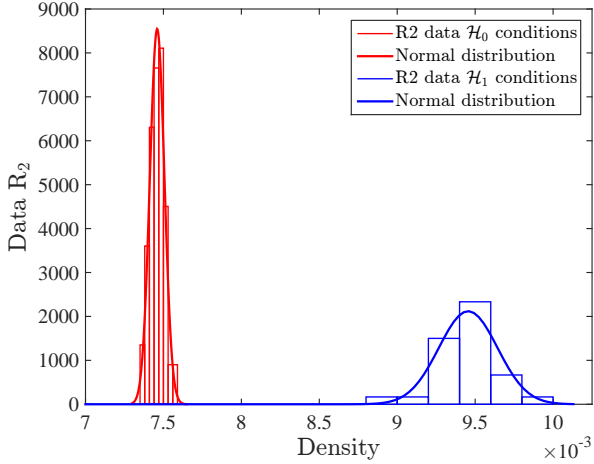


Fig. 8. Histogram of the R_2 EEC parameter in non-faulty and faulty operation. The non-faulty operation R_2 data follows a normal distribution with mean of $\mu_0 = 7.459 \cdot 10^{-3}$ and a variance of $\sigma^2 = 2.179 \cdot 10^{-9}$. The faulty operation R_2 data follows a normal distribution with mean of $\mu_0 = 9.45 \cdot 10^{-3}$ and a variance of $\sigma^2 = 0.188 \cdot 10^{-3}$.

which is shown in Fig. 8 with a red color. The Gaussian distribution is fitted to the data with a mean of $\mu_0 = 7.459 \cdot 10^{-3}$ and a variance of $\sigma^2 = 2.179 \cdot 10^{-9}$.

The best distribution that fits the data of the parameter R_2 , after there is mixed 0.5 % CO into the anode gas, is a Gaussian distribution which is shown in Fig. 8 with blue color. The Gaussian distribution is fitted to the data with a mean of $\mu_0 = 9.45 \cdot 10^{-3}$ and a variance of $\sigma^2 = 0.188 \cdot 10^{-3}$. On the basis of this prior knowledge, the change detection scheme can aim to detect a change in mean with unknown amplitude.

5. DETECTION SCHEME

The statistical change detector will be designed to detect a deviation in the R_2 parameter amplitude, indicating a rise in CO concentration in the anode gas. The detector will be designed based on the experimental data. The problem can therefore be formulated as a one-sided hypothesis test, to detect a change of R_2 with an unknown amplitude, with the null hypothesis (\mathcal{H}_0) as the no-faulty state and the alternative hypothesis (\mathcal{H}_1) as the faulty state.

$$\begin{aligned} \mathcal{H}_0 : R_2 &= \mu_0(\bar{I}) \\ \mathcal{H}_1 : R_2 &> \mu_0(\bar{I}) \end{aligned}$$

Since the test aims to detect a change in mean value of R_2 , but with an unknown amplitude, for an unknown CO concentration, the detector will be a Composite hypothesis testing. Composite hypothesis testing without prior knowledge of the likelihood of whether or not CO pollution is present, is based on the Neumann-Pearson approach and the Generalized Likelihood Ratio Test (GLRT) is employed. (Kay, 1998). When the change has unknown magnitude, the change is estimated by the GLRT using a maximum likelihood estimation (MLE) approach. Based on previous experience, it appears to perform extremely well in technical applications, even though optimality is

not guaranteed for the GLRT.

The first step in the GLRT is to determine the unknown parameter, in this case the amplitude of change of resistance from \mathcal{H}_0 to \mathcal{H}_1 conditions. MLE of the amplitude in a Gaussian signal, is in (Kay, 1993) determined to be the mean of the signal.

The GLRT decision algorithm $g(k)$ detects a rise in the CO concentration, through monitoring of the resistance changes in the fuel cell and decides \mathcal{H}_1 when the $g(k)$ function becomes larger than a threshold γ . Two versions of the GLRT algorithm are tested, one is implemented as shown in Eq. 4 (Blanke et al., 2006) where both change magnitude and instant of change are estimated, the other is Eq. 3, which does not estimate the most likely instant of change. In Eqs. 3 and 4 σ^2 is the variance of R_2 in the non-faulty operation, $\mu_0(\bar{I})$ is the mean value of R_2 in non-faulty operation and obtained as given in Eq. 2, where \bar{I} denotes the steady state current.

The GLR test statistic for detection of a change in mean with unchanged variance before and after the change, and a window size M , reads

$$g(k) = \frac{1}{2\sigma^2 M} \left[\sum_{i=k-M+1}^k (R_2(i) - \mu_0(\bar{I})) \right]^2 \quad (3)$$

A slight variation, which estimates the instant of change, and is more computation heavy, is also tested. The $g_m(k)$ GLRT from (Blanke et al., 2006) is shown in Eq. 4.

$$g_m(k) = \frac{1}{2\sigma^2} \max_{k-M+1 \leq j \leq k} \frac{1}{k-j+1} \left[\sum_{i=j}^k (R_2(i) - \mu_0(\bar{I})) \right]^2 \quad (4)$$

The maximization of $g(k)$ is implemented with a window of size M , as shown in Eq. 3. The window size is chosen as a balance between probability P_D to detect a change of a desired magnitude, and the delay of detection. As seen in Fig. 5, the voltage changes during 2 hours, when a CO contamination is introduced. The window size is therefore chosen to $M = 6$ corresponding to 2 hours.

The test statistic $g(k)$ is shown for the time series of the EEC parameter $R_2(k)$, in Fig. 9. The red line shows the threshold (γ).

It is seen in Fig. 9 that $g_m(k)$ given in Eq. 4 has a slightly faster detection compared with $g(k)$, the two tests are alike outside this transient region. In praxis, therefore, since CO contamination could be imagined to be incipient, the computationally cheaper $g(k)$ could be used.

A probability plot of $g(k)$ is shown in Fig. 11 for the non-faulty \mathcal{H}_0 case. According to (Kay, 1998), the test statistics the square sum of normal distributed random variables that are independent and identically distributed (IID), should follow a χ_ν^2 distribution where ν is the number of parameters being estimated. In our case, $\nu = 1$

The autocorrelation of R_2 is plotted in Fig. 10, which shows samples to be reasonably uncorrelated. However, as seen in Fig. 11 the $g(k)$ data do not follow the theoretical χ_1^2 distribution. The low number of samples in R_2 under \mathcal{H}_0 conditions results in a relatively high whiteness level,

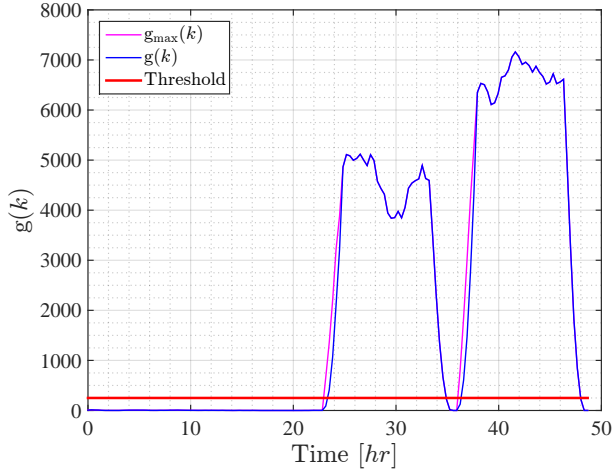


Fig. 9. The GLRT decision algorithm $g(k)$ detecting a change in the mean value of R_2 .

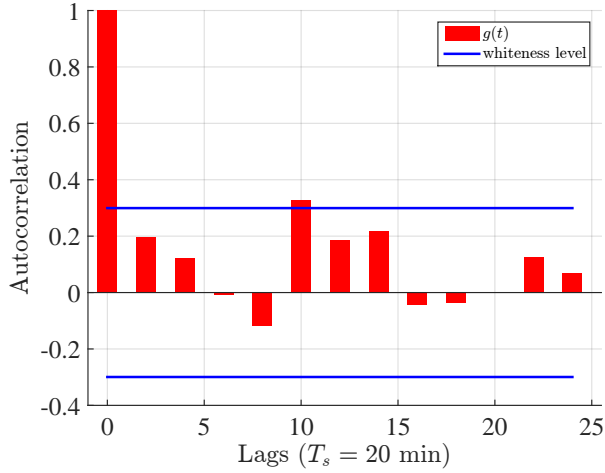


Fig. 10. Autocorrelation for the EEC parameter R_2 under \mathcal{H}_0 conditions.

Table 2. Parameters for the probability distributions fitted to the \mathcal{H}_0 data in Fig. 11.

	μ_{g0}	a	b
Exponential	2.7820		
Gamma		0.7022	3.962

Table 3. Parameters for the probability distributions fitted to the \mathcal{H}_1 data in Fig. 12.

	a	b
Gamma	108.169	42.4392

and the identical distribution of samples has not been experimentally verified. If more samples were available, the whiteness level would be lower, and the indication of independence would change. The test statistics $g(k)$ is therefore fitted to a exponential distribution which provides the best fit of the data, as shown in Fig. 11. The estimated parameters are shown in Table 2.

The threshold (γ) needs to be determined to give an good balance between P_{FA} and P_D . The P_{FA} can be determined from the test statistics for $g(k)$ given in Fig. 11, as $P\{g > \gamma | \mathcal{H}_0\}$. The threshold (γ) is determined by the right tail area of the exponential density function, see

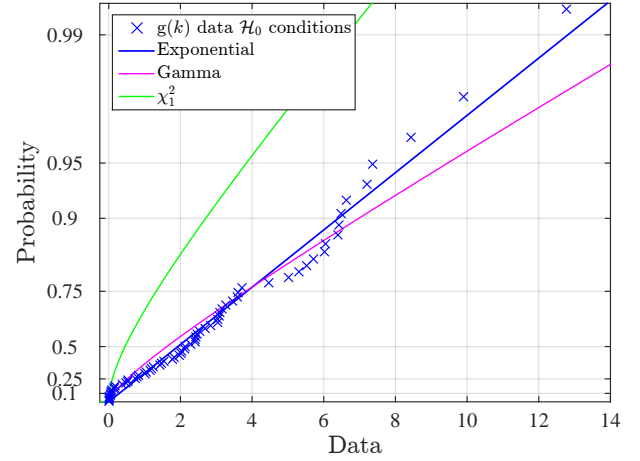


Fig. 11. Probability plot of the data for $g(k)$ compared to different distributions, for \mathcal{H}_0 conditions.

(Kay, 1998) for theoretical results and (Blanke et al., 2012) for discussion of various real-life issues.

$$P_{FA} = P\{g > \gamma | \mathcal{H}_0\} \quad (5)$$

$$= \int_{\gamma}^{\infty} P\{g > \gamma | \mathcal{H}_0\} dg \quad (6)$$

$$= \int_{\gamma}^{\infty} \frac{1}{\mu_{g0}} \exp\left(-\frac{1}{\mu_{g0}} \cdot g\right) dg \quad (7)$$

$$= \exp\left(-\frac{\gamma}{\mu_{g0}}\right) \Leftrightarrow \quad (8)$$

$$\ln(P_{FA}) = \frac{-\gamma}{\mu_{g0}} \Leftrightarrow \quad (9)$$

$$\gamma = -\mu_{g0} \ln(P_{FA}) \quad (10)$$

Designing for an extremely low $P_{FA} = 10^{-39}$, gives $\gamma = 250$. This results in a good detection probability but at the same time a negligible probability of false detection. This is due to a very strong sensitivity of the R_2 parameter to CO contamination and due to low variance on .

A probability plot of $g(k)$ for the faulty \mathcal{H}_1 conditions is shown in Fig. 12 with a Gamma distribution fitted to the data. Furthermore the threshold (γ) is shown in Fig. 12 by a red line. It is clearly seen that the probability of detection is very high, and in practice the probability of detection will be $P_D \approx 1$. A probability of detection of $P_D \approx 1$ indicates that lower rates of CO contamination can be detected.

6. DISCUSSION

This method indicates a strong detectability for CO contamination in the anode gas of a HTPEM fuel cell. The method does not take into account that the fuel cell impedance is changing with catalyst degradation and other degradation mechanisms. Furthermore the fuel cell impedance is dependent on different operating conditions such as the current, temperature, contamination of the anode and cathode gas, etc. as shown in (Andreasen et al., 2011). This method takes the change in current into account and is neglecting other operating conditions. As stated in this paper the temperature is kept constant

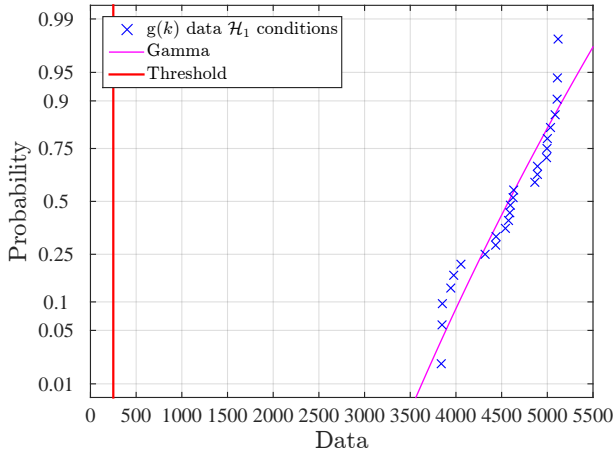


Fig. 12. Probability plot of the $g(k)$ data for \mathcal{H}_1 conditions of 1% CO contamination fitted to a Gamma distribution. The red line shows the threshold ($\gamma = 250$).

during all operation, however in practice this is hard to accomplish. Small temperature variations of the fuel cell will the detection scheme be robust toward, since around the temperature set point is the cell impedance only varying within small limits. (Andreasen et al., 2009) It is suggested to be investigated further what effect the degradation and change in other operating conditions will have on the EEC parameters, so the mapping of the EEC parameters done in Fig. 4, can be expanded if necessary to take these phenomena into account.

The fault is introduced as step in the CO gas flow. In real life the introduction of CO will happen with some dynamic and therefore not as a step. However the GLRT detection scheme detects a change in the amplitude of the R_2 parameter and can therefore also detect incipient faults.

7. CONCLUSION

This paper has shown design and empirical verification of a detection scheme to diagnose CO contamination in the anode gas of a high temperature PEM fuel cell. The data was experimentally determined impedance that was used to estimate parameters in an electrical equivalence model. The equivalence circuit was a simplified Randle's circuit, which was found sufficient for the purpose. A differential evolution optimization method was used to fit impedance data to the electrical equivalent circuit model. The method that uses the change in impedance as a function of varying load current was found effective for the purpose. A generalized likelihood ratio change detection test was designed to detect possible CO contamination. The method showed very high detectability for the 0.5% CO concentration used in experiments, with a negligible probability of false alarms. The detection method promise very high sensitivity of contamination. Further investigation of the change in impedance as function of fuel cell degradation and other impedance dependencies, and also effects of contamination with other than CO need be investigated before the

method could be implemented in full scale applications.

REFERENCES

- Andreasen, S.J., Jespersen, J.L., Schaltz, E., and Kær, S.K. (2009). Characterisation and modelling of a high temperature pem fuel cell stack using electrochemical impedance spectroscopy. *Fuel Cells*, 463–473.
- Andreasen, S.J., Vang, J.R., and Kær, S.K. (2011). High temperature pem fuel cell performance with co and co2 using electrochemical impedance spectroscopy. *International journal of hydrogen energy*, 36, 9815–9830.
- Araya, S.S., Andreasen, S.J., and Kær, S.K. (2012). Experimental characterization of the poisoning effects of methanol-based reformate impurities on a pbi-based high temperature pem fuel cell. *Energies*, 5, 4251–4267.
- Beer, C., Barendse, P., Pillay, P., Bullecks, B., and Rengaswamy, R. (2013). Electrical circuit analysis of co poisoning in high temperature pem fuel cells for rapid fault diagnostics. In *Energy Conversion Congress and Exposition (ECCE), 2013 IEEE*, 4623–4630.
- Blanke, M., Fang, S., Galeazzi, R., and Leira, B.J. (2012). Statistical change detection for diagnosis of buoyancy element defects on moored floating vessels. In *Proc. IFAC Safeprocess 2012, Mexico*, 462–467.
- Blanke, M., Kinnaert, M., Lunze, J., and Staroswiecki, M. (2006). *Diagnosis and Fault-Tolerant Control*. Springer, 2nd edition.
- Ellis, M.W., Spakovsky, M.R.V., and Nelson, D.J. (2001). Fuel cell systems: Efficient, flexible energy conversion for the 21st century. *Proc. of the IEEE*, 89(12), 1808–1818.
- Jensen, H.C.B., Andreasen, S.J., Kær, S.K., and Schaltz, E. (2013). Estimation of co concentration in high temperature pem fuel cells using electrochemical impedance. *Proceedings of the 5th International Conference on Fundamentals and Development of Fuel Cells*.
- Justesen, K.K., Andreasen, S.J., Shaker, H.R., Ehmsen, M.P., and Andersen, J. (2013). Gas composition modeling in a reformed methanol fuel cell system using adaptive neuro-fuzzy inference systems. *International Journal of Hydrogen Energy*, 38, 10577–10584.
- Kay, S.M. (1993). *Fundamentals of Statistical Signal Processing - Volume I Estimation Theory*. Prentice Hall PTR.
- Kay, S.M. (1998). *Fundamentals of Statistical Signal Processing - Volume II Detection Theory*. Prentice Hall.
- Lottin, O., Antoine, B., Colinart, T., Didierjean, S., Maranzana, G., Moyne, C., and Ramousse, J. (2009). Modelling of the operation of polymer exchange membrane fuel cells in the presence of electrodes flooding. *International Journal of Thermal Sciences*, 48, 133–145.
- Storn, R. and Price, K. (1997). Differential evolution - a simple and efficient heuristic for global optimization over continuous spaces. *Journal of Global Optimization*, 11, 341–359.
- Yang, G. (2014). Battery parameter estimation based on differential evolution via boundary evolution strategy. *International Journal Power Sources*, 245, 583–593.